Journal of Integrative Neuroscience

J. Integr. Neurosci. **2026**; 25(9): 50741
https://doi.org/10.31083/JIN50741

Original Research

Esketamine Ameliorates Propofol-Induced Long-Term Cognitive Impairments in Juvenile Rats by Suppressing Autophagy via Activating the PI3K/Akt/mTOR Signaling Pathway

Yang Wang[1], Yin Li[1], Zhe Chen[1], Xuexue Zhang[1], Na Qi[2], Xueying Chen[1], Guiping Xu[1,*]

[1]Department of Anesthesia, People's Hospital of Xinjiang Uygur Autonomous Region; Xinjiang Clinical Research Center for Anesthesia Management, 830000 Urumqi, Xinjiang, China
[2]Graduate School of Xinjiang Medical University, 830000 Urumqi, Xinjiang, China
*Correspondence: xgpsyl@126.com (Guiping Xu)
Academic Editor: Ahmad Khundakar
Submitted: 5 February 2026 Revised: 10 July 2026 Accepted: 24 July 2026 Published: 21 September 2026

Abstract

Background: Repeated propofol exposure during neurodevelopment induces long-term cognitive deficits in rats, potentially through dysregulated hippocampal neuronal autophagy and inhibition of the phosphatidylinositol 3-kinase (PI3K)/protein kinase B (Akt)/mechanistic target of rapamycin (mTOR) pathway. Esketamine has been reported to exert neuroprotective effects; however, the underlying mechanism remains unclear. In the present study, we investigated whether esketamine could ameliorate propofol-induced long-term memory and learning impairments in juvenile rats by suppressing autophagy via activation of the PI3K/Akt/mTOR pathway. **Methods:** Seventy-two Sprague-Dawley rats of both sexes at postnatal day 7 were randomly assigned to one of six groups: Control, Propofol, Esketamine + Propofol, LY294002 (PI3K inhibitor) + Esketamine + Propofol, Rapamycin + Propofol, and Rapamycin + Esketamine + Propofol. All treatments were administered daily for five consecutive days. Cognitive performance was assessed using both the Y-maze test and the Morris water maze test. Hippocampal neuronal pathology was evaluated by histopathological staining and transmission electron microscopy. The concentrations of pro-inflammatory cytokines and expression levels of proteins related to the PI3K/Akt/mTOR pathway and autophagy were measured using Western blotting and immunofluorescence. **Results:** Rats exposed to propofol showed significant learning and memory impairments, hippocampal neuronal damage, suppression of the PI3K/Akt/mTOR pathway, excessive autophagy, and elevated levels of pro-inflammatory cytokines ($p < 0.01$). Esketamine co-treatment significantly alleviated these propofol-induced changes ($p < 0.01$). However, the neuroprotective effects of esketamine were diminished by pre-treatment with either LY294002 or the autophagy activator rapamycin ($p < 0.01$). **Conclusion:** Esketamine ameliorates propofol-induced long-term cognitive impairments in juvenile rats by suppressing excessive autophagy through activation of the PI3K/Akt/mTOR signaling pathway.

Keywords: autophagy; esketamine; mechanistic target of rapamycin; propofol; protein kinase B; phosphatidylinositol 3-kinase; rats

1. Introduction

The widespread use of general anesthetics in pediatric surgery has raised significant concerns regarding their potential neurotoxicity [1]. Accumulating evidence has demonstrated that early exposure to general anesthesia may be associated with neurobehavioral developmental disorders, cognitive decline, and long-term brain injury [2,3]. While a single, short-term anesthetic exposure may not result in detectable neurodevelopmental effects, multiple or prolonged exposures are more likely to lead to adverse outcomes [4]. Propofol, a commonly used intravenous anesthetic, has been extensively studied for its safety and potential impact on neurodevelopment. Studies demonstrated that repeated or prolonged propofol exposure can cause long-term alterations in hippocampal function in developing brains, subsequently impairing learning and memory capabilities [5,6,7]. Consequently, recent investigations using animal models have sought to elucidate the molecular mechanisms of propofol-induced neurotoxicity and to identify potential interventions, thereby improving neurodevelopmental outcomes.

As a major intracellular degradation and recycling process, autophagy is essential for neuronal function and homeostasis [8]. Accumulating evidence links autophagy to cognitive processes, including learning and memory [9,10]. The impact of propofol on cognitive function is closely related to its modulation of autophagy. While moderate activation of autophagy may be noteworthy, its dysregulation can contribute to cognitive impairment. Preclinical research demonstrated that propofol could enhance hippocampal neuronal autophagy during development, leading to cognitive deficits [11]. Furthermore, the interaction between autophagy and other cellular processes, including apoptosis, ferroptosis, oxidative stress, and inflammation, significantly influences cognitive function [12].

Esketamine (the S-enantiomer of ketamine) is a non-competitive N-methyl-D-aspartate (NMDA) receptor an-

Copyright: © 2026 The Author(s). Published by IMR Press.
This is an open access article under the CC BY 4.0 license.

Publisher's Note: IMR Press stays neutral with regard to jurisdictional claims in published maps and institutional affiliations.

tagonist. As a relatively recent anesthetic agent, it is utilized not only for sedation, but also for its potent analgesic effects [13]. Its sympathomimetic properties serve to counteract the hemodynamic depression induced by propofol, potentially mitigating cardiovascular and respiratory risks, thereby making it appropriate for a broad range of surgical procedures and rapid diagnostic examinations [14,15]. Beyond its anesthetic applications, esketamine has demonstrated rapid antidepressant efficacy [16], and it is implicated in enhancing neuronal plasticity [17], modulating neuronal activity [18], and exerting neuroprotective effects [19]. Recent research in rats demonstrated that esketamine can mitigate propofol-induced brain injury and cognitive dysfunction [20]. Moreover, a recent investigation revealed that esketamine ameliorates propofol-induced cognitive impairment in aged rats by modulating neuronal autophagy [21]; however, the precise mechanism varies depending on the pathological context and specific signaling pathways involved.

The phosphatidylinositol 3-kinase (PI3K)/protein kinase B (Akt)/mechanistic target of rapamycin (mTOR) pathway is a key autophagy regulator, whose activation typically suppresses autophagic activity and helps maintain neuronal homeostasis [22]. Notably, an earlier study found that esketamine relieved neuropathic pain and enhanced autophagy through PI3K/Akt/mTOR inhibition [23], highlighting the context-dependent nature of esketamine's actions. Nevertheless, it remains elusive whether, in the developing brain, esketamine suppresses propofol-induced excessive neuronal autophagy by activating the PI3K/Akt/mTOR signaling pathway, thereby improving long-term learning and memory deficits. Therefore, the present study aimed to explore whether esketamine could ameliorate long-term memory and learning impairments following propofol anesthesia in juvenile rats by activating the PI3K/Akt/mTOR pathway and subsequently inhibiting hippocampal neuronal autophagy.

2. Materials and Methods

2.1 Animals

Seventy-two clean, healthy postnatal day 7 (P7) Sprague-Dawley rats, irrespective of sex, weighing 10–15 g, were obtained from the Animal Center of Xinjiang Medical University (Xinjiang, China). All animals were housed under specific pathogen-free conditions in a well-ventilated environment maintained at 21–26 °C under a 12/12-h light/dark cycle with 30–60% humidity. Pups were kept with their dams until weaning at postnatal day 21 and then group-housed (n = 3 per cage). All animals had free access to water and food. The animal experiments were conducted following the Animal Research: Reporting of In Vivo Experiments (ARRIVE) 2.0 guidelines (**Supplementary Materials-ARRIVE**) and the National Institutes of Health (NIH) standards for laboratory animal welfare. All experimental procedures were performed at the Animal Center of Xinjiang Medical University (Xinjiang, China).

2.2 Groups and Treatments

In total, 72 rats were randomly allocated to six groups (n = 12 per group) using a computer-generated random number sequence:

(1) Control group (Con): Saline (100 mg/kg) was administered to the rats by intraperitoneal (i.p.) injection.

(2) Propofol group (Pfo): A propofol neurotoxicity model was established as previously reported [24]. Rats were administered propofol (50 mg/kg, i.p.; Xi'an Libang Pharmaceutical Co., Ltd., Xi'an, Shaanxi, China; catalog No. H19990282). Following the return of the righting reflex (30–60 min after the first propofol injection), an additional dose of propofol (50 mg/kg, i.p.) was subsequently administered.

(3) Esketamine + Propofol group (Esk+Pfo): Rats received an injection of esketamine (10 mg/kg, i.p.; Jiangsu Hengrui Medicine Co., Ltd., Lianyungang, Jiangsu, China; catalog No. H20193336). Thirty minutes later, the first dose of propofol (50 mg/kg, i.p.) was administered. After recovery of the righting reflex (30–60 min after the first propofol injection), a second dose of propofol (50 mg/kg, i.p.) was administered.

(4) PI3K inhibitor LY294002 + Esketamine + Propofol group (LY294002+Esk+Pfo): The PI3K inhibitor LY294002 was administered intraperitoneally at 10 mg/kg [25]. Thirty minutes later, esketamine (10 mg/kg, i.p.) was administered. Thirty minutes after the esketamine injection, the first dose of propofol (50 mg/kg each) was administered. After recovery of the righting reflex (30–60 min later), a second propofol dose (50 mg/kg, i.p.) was administered.

(5) Autophagy activator Rapamycin + Propofol group (Rapa+Pfo): Rats received an i.p. injection of the autophagy activator rapamycin (7.5 mg/kg) [26]. Thirty minutes later, the first dose of propofol (50 mg/kg, i.p.) was administered. After recovery of the righting reflex (approximately 30–60 min after the first propofol injection), a second dose of propofol (50 mg/kg, i.p.) was administered.

(6) Autophagy activator Rapamycin + Esketamine + Propofol group (Rapa+Esk+Pfo): Rats received an i.p. injection of rapamycin (7.5 mg/kg). Thirty minutes later, esketamine (10 mg/kg, i.p.) was administered. After recovery of the righting reflex (30–60 min later), a second propofol dose (50 mg/kg each) was administered.

All treatments were administered at a consistent time daily for five consecutive days. Immediately following each injection, neonatal rats were placed in an incubator (Thermo Fisher Scientific, Waltham, MA, USA) maintained at 37 °C, with 100% oxygen supplied at a flow rate of 2 L/min. Respiratory status was closely monitored throughout the anesthetic period, including respiration rate and the color of the skin and mucous membranes. In addi-

tion, oxygen saturation was continuously monitored using a MouseOx® Plus pulse oximeter (Starr Life Sciences Corp., Oakmont, PA, USA) and remained above 95% in all experimental groups. Animals were observed until complete restoration of the righting reflex to ensure safety before being returned to their dams. No deaths, cyanosis, or abnormal recovery patterns were observed during the treatment period.

2.3 Working Memory Assessment Using the Y-Maze Test

The Y-maze test was performed to assess working memory on postnatal day 30 (P30). The Y-maze, one of the most straightforward paradigms, is widely utilized to evaluate learning and memory capabilities in rodents [27]. The apparatus consists of three arms; each fitted with electrifiable copper grids. One arm was randomly designated as the start compartment. Another arm was designated as the safe compartment, defined by constant illumination and the absence of foot shocks throughout the test. The third arm was designated as the non-safe compartment, characterized by being unlit and equipped with a grid floor for delivering foot shocks during the training phase. Foot shocks (0.3 mA intensity, 2-sec duration) were delivered via the grid floor upon entry into the non-safe compartment.

During the training phase, a foot shock was delivered after a 5-sec delay following the illumination of the safe compartment. An escape to the safe compartment was recorded as a correct response. The learning criterion was defined as achieving nine consecutive correct responses. Before testing, animals were allowed to freely explore the maze for 3 min. The voltage intensity was adjusted to ensure escape behavior within a 10-sec window. The number of training trials to criterion was recorded for each rat. Notably, 23 h later, memory retention was assessed by administering 20 consecutive trials. The correct response rate (%) was calculated as $\frac{\text{number of correct responses}}{20} \times 100\%$. All experiments were conducted during a fixed time window (9:00–12:00) under controlled conditions of 50 lux illumination and <35 dB background noise.

The investigators responsible for the Y-maze test were blinded to the treatment allocation.

2.4 Assessment of Spatial Memory by Morris Water Maze (MWM) Test

Spatial learning and memory were assessed on postnatal day 60 using the MWM. The MWM apparatus consisted of a circular stainless-steel pool measuring 1.2 m in diameter, with the water temperature maintained at 25 ± 1 °C. A hidden platform (diameter: 9 cm) was positioned in the center of the second quadrant, 2 cm beneath the water surface. Distinct visual cues placed around the testing room served as spatial references during navigation. The test comprised two consecutive phases: acquisition phase (days 1–5): Rats underwent four training trials daily for five consecutive days. In each trial, the animal was released into the water from one of four starting points facing the wall, corresponding to the four quadrants, in a clockwise sequence each day. A 10-min inter-trial interval was enforced. The time taken to locate the hidden platform in each trial was recorded as the escape latency (s). If a rat could not find the platform within 120 sec, it was guided to the platform, and the escape latency was recorded as 120 sec.

Probe trial (day 6): In this phase, 24 h after the final acquisition session, a probe trial was employed to assess long-term spatial memory. The hidden platform was removed from the pool, and each animal was allowed to freely swim for 120 sec. Throughout this interval, crossings over the former platform site were counted and recorded.

The MWM test was performed during a fixed time window (9:00–12:00) under standardized conditions of 50 lux illumination and background noise of below 35 dB. For data recording, the escape latency during these guided trials was consistently recorded as 120 sec when the animal did not escape within the allotted time. In the statistical analysis, all latency values, including those recorded as 120 sec, were included in the analysis without exclusion or special weighting.

Treatment assignments were concealed from the investigators conducting the MWM assessment.

2.5 Histopathological Assessment of Neuronal Injury in the Hippocampus

Following behavioral tests, rats were anesthetized with 2% sodium pentobarbital (50 mg/kg, i.p.; Sigma-Aldrich, St. Louis, MO, USA; catalog No. P3761) and subsequently euthanized by decapitation. The brain was removed rapidly, and hippocampal tissue was dissected on ice. Tissue blocks containing the hippocampal Cornu Ammonis area 1 (CA1) region (thickness ≤0.5 cm) were fixed at room temperature in 10% neutral buffered formalin for 23 h.

After fixation, samples were dehydrated through a graded ethanol series, cleared, and then embedded in paraffin (Sinopharm Group Chemical Reagent Co., Ltd., Shanghai, China; catalog No. 69019361). Coronal paraffin sections (5 μm thick) were prepared using a microtome (Leica Microsystems, Wetzlar, Germany) and subsequently processed for hematoxylin and eosin staining kit (Solarbio, Beijing, China; catalog No. G1120). Sections were first exposed to hematoxylin for 10 min, differentiated in 1% acid alcohol for 50 sec, and then counterstained with eosin for 5 min. Finally, the sections were dehydrated and cleared, followed by mounting with neutral balsam (Nanchang Yulu Experimental Equipment Co., Ltd., Nanchang, Jiangxi, China; catalog No. 20200237).

Light-microscopic evaluation of the stained sections was performed at 300× magnification using an Axio Imager A2 microscope (Carl Zeiss AG, Oberkochen, Germany). Two blinded investigators independently evaluated neuronal damage in the hippocampal CA1 region. Brain

injury scores were assigned on the basis of standardized criteria that assessed morphological changes, such as pyknosis, neuronal loss, and eosinophilic cytoplasm. Specifically, scores were assigned on the basis of a 0–10 semi-quantitative scale, as previously described for hippocampal pyramidal neuron injury assessment, in which the percentage of CA1 neuronal loss is represented on a 0–10 scale: 0 = no injury; 1–2 = minimal injury (<20% affected neurons); 3–4 = mild injury (20–35%); 5–6 = moderate injury (35–55%); 7–8 = severe injury (55–75%); 9–10 = very severe injury (>75%). Two blinded investigators independently evaluated five non-overlapping fields per section (300× magnification), and the mean score was calculated for each rat [28].

2.6 Ultrastructural Examination of Hippocampal CA1 Neurons and Autophagosomes (APs) by Transmission Electron Microscopy (TEM)

Hippocampal tissue was fixed in 2.5% glutaraldehyde (Servicebio Technology, Wuhan, Hubei, China; catalog No. G1102) at 3 °C for 23 h before being processed as follows: samples were rinsed three times (15 min each) with 0.1 M phosphate buffer, followed by post-fixation with 1% osmium tetroxide (Ted Pella Inc., Redding, CA, USA; catalog No. 18456) for 2 h. The specimens were subsequently dehydrated through a graded acetone series (50%, 70%, and 90%, 15 min each; Sinopharm Group Chemical Reagent Co., Ltd., Shanghai, China; catalog No. 10000418), immersed three times in 100% acetone (20 min each), embedded in epoxy resin (SPI Supplies, West Chester, PA, USA; catalog No. 90529-77-4), infiltrated overnight, and polymerized at 60 °C for 38 h. Ultrathin sections (thickness: 70 nm) were prepared and stained for 30 min with uranyl acetate (Ted Pella Inc., Redding, CA, USA; catalog No. NC1630603), followed by lead citrate (Ted Pella Inc., Redding, CA, USA; catalog No. 19312) for 15 min.

Hippocampal CA1 neuronal ultrastructure was examined at 8000× magnification with an HT7800 transmission electron microscope (Hitachi, Tokyo, Japan). For quantitative analysis, six rats per group were randomly selected, and 5–10 non-overlapping fields per rat were photographed. All microscopic tests were independently performed by two researchers blinded to treatment allocation. Identification of APs strictly adhered to the international guidelines [29]. APs were defined as double-membraned vesicles, with a diameter ranging from 0.5 to 1.5 µm, containing cytoplasmic components, such as undegraded organelles (e.g., mitochondria and fragments of the endoplasmic reticulum). Secondary lysosomes and multivesicular bodies (MVBs) were explicitly excluded from this classification.

Autophagic vacuoles were identified and quantified based on their ultrastructural morphology. APs were defined as double-membraned crescent-shaped or circular vesicles that enclosed cytoplasmic contents (e.g., organelles). Autolysosomes (ALs) were characterized as single-membrane structures containing electron-dense material at various stages of degradation. The identification and counting of these vacuoles were performed independently by two investigators, both blinded to treatment allocation. The total number of autophagic vacuoles (AVs) per microscopic field was determined by summing the counts of APs and ALs.

2.7 Quantification of Hippocampal Cytokines by Enzyme-Linked Immunosorbent Assay (ELISA)

The levels of interleukin (IL)-1β, IL-6, IL-18, and tumor necrosis factor-α (TNF-α) in hippocampal tissues were quantified using commercially available ELISA kits (Solarbio, Beijing, China): IL-1β (catalog No. SEKR-0002), IL-6 (catalog No. SEKR-0005), IL-18 (catalog No. SEKR-0054), and TNF-α (catalog No. SEKR-0009). In brief, approximately 50 mg of tissue was homogenized in ice-cold physiological saline and centrifuged at 3 °C for 10 min at 12,000 ×g to collect the supernatant. Standard curves were generated using serially diluted standards according to the manufacturer's instructions. Both samples and standards were incubated in pre-coated wells. The assay procedure involved sequential incubation with a biotinylated detection antibody, streptavidin-conjugated horseradish peroxidase (HRP), and tetramethylbenzidine substrate. The absorbance at 350-nm wavelength was measured. The final cytokine concentrations in the tissue homogenate supernatant were expressed as ng/L.

2.8 Western Blotting

Hippocampal tissue was flash-frozen in liquid nitrogen and minced. The fragments were homogenized in ice-cold radioimmunoprecipitation assay (RIPA) lysis buffer (Meilunbio, Dalian, Liaoning, China; catalog No. MA0151) containing phosphatase/protease inhibitors at a 1:10 (w/v) tissue-to-buffer ratio. Mechanical homogenization was performed under ice-cold conditions with three cycles of 30-sec homogenization interspersed with 60-sec cooling intervals. Centrifugation of the homogenates was conducted at 16,200 ×g for 15 min at 3 °C (centrifugal radius, 10 cm). The supernatant was retained as the total protein fraction, and protein concentration was quantified by a bicinchoninic acid assay. Protein samples (50 µg per lane) were separated by 12% sodium dodecyl sulfate-polyacrylamide gel electrophoresis SDS-PAGE (Sinopharm Group Chemical Reagent Co., Ltd., Shanghai, China; SDS catalog No. 30166428) for 1.5 h at a constant voltage of 120 V. Subsequently, proteins were transferred onto 0.35 µm polyvinylidene fluoride membranes (0.35 µm; Merck Millipore, Billerica, MA, USA; catalog No. IPVH00010) using a wet transfer system (Genscript, Nanjing, Jiangsu, China; catalog No. L00686C) for 90 min at constant 300 mA. The membranes were blocked at room temperature with 5% skim milk (Servicebio, Wuhan, Hubei, China; catalog No. G5002) for 1

h and then incubated overnight at 3 °C with the corresponding primary antibodies (Servicebio; diluted 1:1000), including PI3K, Akt, mTOR, phosphorylated-PI3K (p-PI3K), phosphorylated-Akt (p-Akt), p-mTOR (p-mTOR), Microtubule-associated protein 1A/1B-light chain 3 (LC3), p62, Beclin-1, and glyceraldehyde-3-phosphate dehydrogenase (GAPDH). Membranes were thrice washed (each 10 min) with Tris-buffered saline with Tween (TBST) after warming to room temperature for 30 min and incubated with HRP-conjugated goat anti-rabbit secondary antibody (Servicebio, Wuhan, Hubei, China; catalog No. GB23303; 1:5000) for 1 h at room temperature. Following additional TBST washing, protein bands were visualized using an enhanced chemiluminescence substrate (Thermo Fisher Scientific, Waltham, MA, USA; catalog No. 32106). Signal detection was performed using a ChemiDoc MP Imaging System (Bio-Rad Laboratories Inc., Hercules, CA, USA), and band intensities were quantified through Image Lab 6.1 (Bio-Rad Laboratories Inc.). The expression of target proteins was normalized to GAPDH. The activity of phosphorylated proteins was expressed as the ratio of the phosphorylated protein to the total protein (p-protein/total protein).

2.9 Immunofluorescence Staining and Analysis

A tyramide signal amplification (TSA)-based multiplex fluorescence staining propofol was employed for dual-labeling of hippocampal sections. After paraffin removal and tissue rehydration, antigen retrieval was achieved by heating the sections in EDTA buffer (pH 9.0; EDTA buffer (pH 9.0; Abcam, Cambridge, UK; catalog No. AB93684)) at 95 °C. 3% H_2O_2 was used to block endogenous peroxidase, after which nonspecific binding was blocked with normal goat serum (Boster Biological Technology, Wuhan, Hubei, China; catalog No. AR1009). Tissue sections were initially incubated overnight at 3 °C with a rabbit monoclonal antibody against microtubule-associated protein 1A/1B-light chain 3B (LC3B, Cell Signaling Technology, Danvers, MA, USA; catalog No. 3868T; 1:1000). Signal amplification was achieved using the appropriate HRP-conjugated secondary antibody (Servicebio Technology, Wuhan, Hubei, China; catalog No. GB23303) and TYR-520Plus fluorescent dye (excitation/emission: 390/520 nm; Ruchuang Biotech, Shanghai, China; catalog No. RC0086Plus-34RM). For subsequent labeling, antibody elution was performed using an antigen retrieval buffer. Sections were thereafter incubated with rabbit anti-lysosomal-associated membrane protein 1 (LAMP1) polyclonal antibody (Bioss, Beijing, China; catalog No. bs-1970R; 1:1000) under identical conditions, followed by visualization with TYR-570Plus fluorescent dye (excitation/emission: 550/570 nm; Ruchuang Biotech, Shanghai, China; catalog No. RC0086Plus-34RM). Nuclei were counterstained with 4′,6-diamidino-2-phenylindole (DAPI; Beyotime Biotechnology, Shanghai, China; catalog No. C1002). All fluorescence images were acquired by a Nikon fluorescence microscope (Nikon, Tokyo, Japan) under consistent parameters. For each group, at least three randomly selected rats were analyzed, involving three non-overlapping fields of view captured from the hippocampal CA1 region per rat (300× magnification). Semi-quantitative analysis of LC3B and LAMP1 fluorescence signals was performed using Image-Pro Plus 6.0 (Media Cybernetics, Rockville, MD, USA). The mean fluorescence intensity was obtained by measuring the integrated optical density and area for each field of view. The final value for each sample represents the average of measurements taken from three fields.

2.10 Statistical Analysis

Continuous data were expressed as mean ± standard deviation. For the MWM acquisition phase (escape latency), a two-way repeated-measures ANOVA (group × day) was performed. For all other comparisons (e.g. platform crossings, Y-maze test, Western blotting), one-way ANOVA followed by Tukey's post-hoc test was used; when assumptions were not met, the Kruskal-Wallis test was applied. The homogeneity of variances and assumptions of normality were assessed separately for each continuous outcome measure (e.g., escape latency, platform crossings) using the Levene's test and the Shapiro-Wilk test, respectively. If either the normality or homoscedasticity assumption was violated, the non-parametric Kruskal-Wallis H test was alternatively utilized. For categorical data, the Chi-square test was applied. The Fisher's exact test was used in cases where the expected frequencies were <5. Statistical significance was determined when a two-tailed p-value was <0.05. Statistical analysis was carried out using SPSS 26.0 software (IBM Corp, Armonk, NY, USA). Individual data points are displayed in all graphs. The behavioral tests and histological evaluation were entirely conducted under blinded conditions. Original datasets were stored on institutional servers and are available upon reasonable request in accordance with academic practice.

3. Results

3.1 Esketamine Ameliorated Long-term Memory and Learning Deficits

Behavioral testing demonstrated that esketamine attenuated propofol-induced long-term cognitive deficits. In the Y-maze test (Fig. 1A,B), rats in the Pfo group required significantly more training trials and showed a significantly lower correct response rate than controls (both $p < 0.01$), indicating impaired learning and memory. Esketamine significantly improved both measures ($p < 0.01$ vs. Pfo), whereas co-administration of LY294002 (PI3K inhibitor) or rapamycin (autophagy activator) abolished these improvements. The LY294002+Esk+Pfo and Rapa+Esk+Pfo groups exhibited no between-group differences, while their performance on all key metrics was significantly worse than that in the Esk+Pfo group ($p < 0.01$).

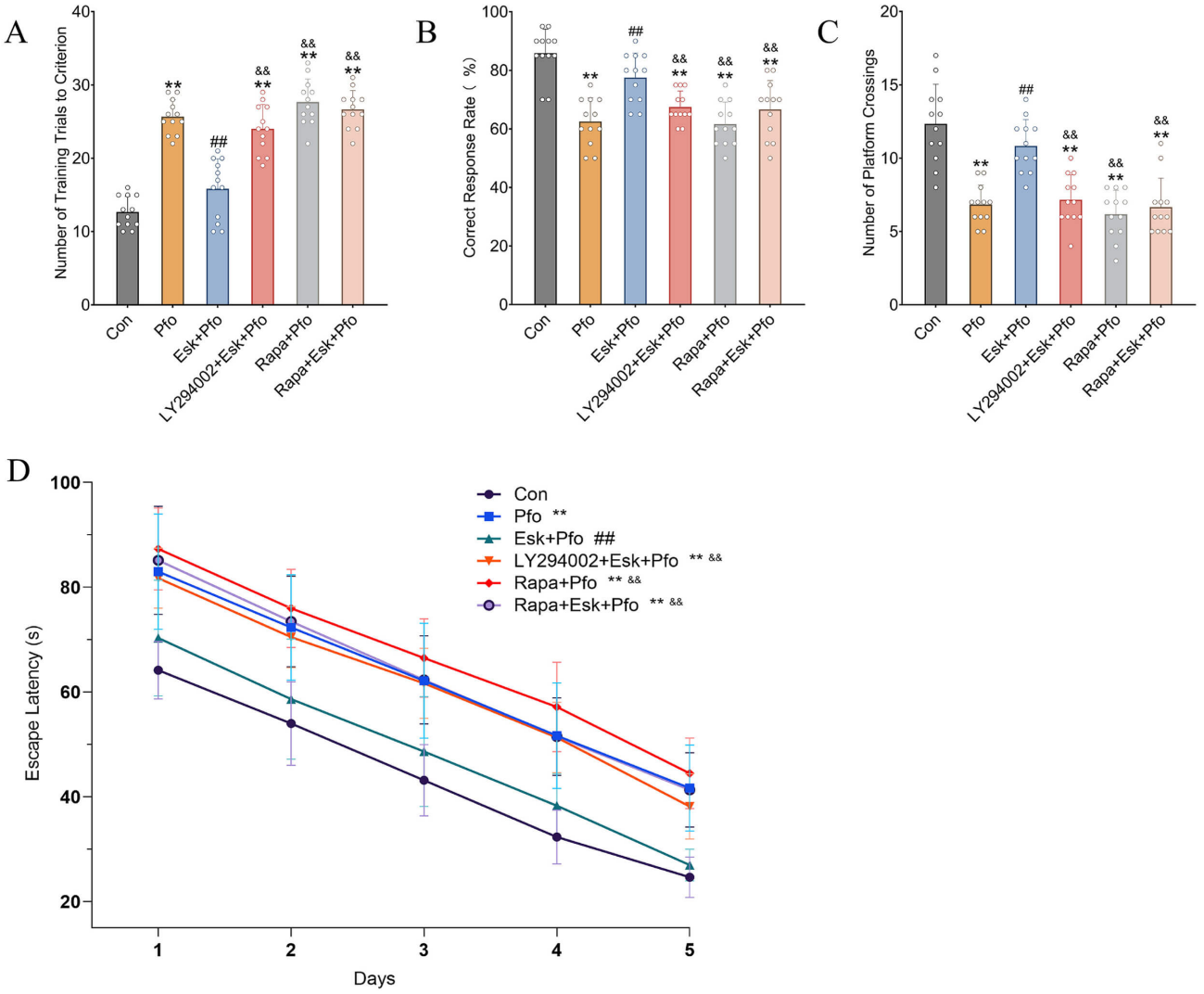

Fig. 1. Esketamine could ameliorate propofol-induced long-term learning and memory impairments, as evidenced by the Y-maze and Morris water maze tests. (A) Number of training trials required to reach the learning criterion. (B) Correct response rate (%). (C) Number of platform crossings. (D) Escape latency (s). (A–C) One-way ANOVA with Tukey's test; (D) Two-way repeated-measures ANOVA with Tukey's test. Data were presented as mean ± SD (n = 12). $^{**}p < 0.01$ vs. Con; $^{\#\#}p < 0.01$ vs. Pfo; $^{\&\&}p < 0.01$ vs. Esk+Pfo. SD, standard deviation; Con, Control group; Pfo, Propofol group; Esk, Esketamine; Rapa, Rapamycin.

Consistent findings were obtained using the MWM test (Fig. 1). Propofol significantly reduced platform crossings in the probe trial (Fig. 1C, $p < 0.01$) and prolonged escape latency during the 5-day acquisition phase (Fig. 1D, $p < 0.01$) compared with the Con group. Esketamine (Esk+Pfo group) markedly improved spatial learning and memory performance ($p < 0.01$), whereas these protective effects were abolished when co-administered with LY294002 or rapamycin. The LY294002+Esk+Pfo and Rapa+Esk+Pfo groups exhibited no significant difference over the Pfo group on either measure and performed significantly worse than the Esk+Pfo group ($p < 0.01$).

Collectively, esketamine could alleviate propofol-induced cognitive impairment, and this protective effect was abolished by either PI3K inhibition or autophagy activation. These results indicate a mechanism dependent on activation of the PI3K/Akt/mTOR pathway and suppression of excessive autophagy.

3.2 Histopathological Assessment of Hippocampal Neuronal Structure by H&E Staining

Histopathological changes in hippocampal neurons were assessed by H&E staining (Fig. 2A). Compared with the well-preserved neuronal architecture observed in the Con group, the Pfo group exhibited remarkable pathological changes, including disorganized neuronal arrangement, cell dispersion (black arrow), and increased glial cell density (yellow arrow). These abnormalities were partially reversed by esketamine treatment. The protective effect of esketamine was significantly attenuated by co-administration

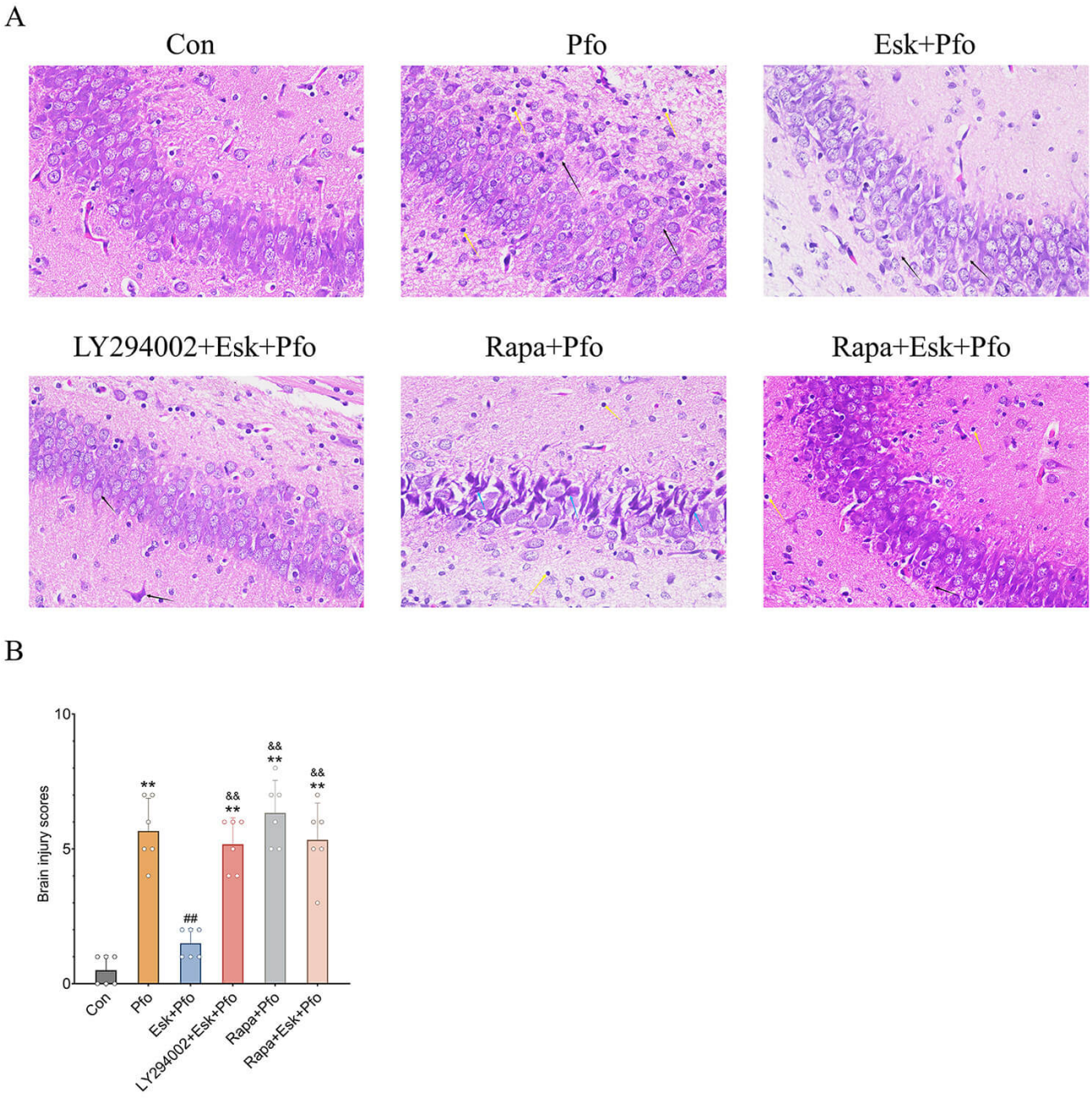

Fig. 2. Neuroprotective effects of esketamine against propofol-induced neurotoxicity. (A) Representative H&E staining images of the hippocampal CA1 region from each group. Black arrows indicate neuronal dispersion with unclear boundaries; blue arrows indicate neuronal pyknosis with cytoplasmic eosinophilia; yellow arrows indicate increased glial cell density. Scale bar: 50 μm (300× magnification). (B) Semi-quantitative histopathological scores. Data were presented as mean ± SD (n = 6). $^{**}p < 0.01$ vs. Con; $^{\#\#}p < 0.01$ vs. Pfo; $^{\&\&}p < 0.01$ vs. Esk+Pfo. H&E, hematoxylin and eosin; CA1, Cornu Ammonis area 1.

of LY294002 or rapamycin. Both the LY294002+Esk+Pfo and Rapa+Esk+Pfo groups displayed severe neuronal damage comparable to the Pfo group, including cell dispersion and pyknosis. The Rapa+Pfo group similarly exhibited remarkable neuronal abnormalities, including nuclear condensation (blue arrow), cytoplasmic eosinophilia, structural disorganization, and glial proliferation, with injury severity comparable to the Pfo group. Semi-quantitative histopathological scores (Fig. 2B) confirmed these findings, reflecting significant protection by esketamine that was abolished by either LY294002 or rapamycin ($p < 0.01$).

Collectively, these histopathological findings demonstrated that esketamine attenuated propofol-induced structural damage in hippocampal neurons, and this protective effect was reversed by either PI3K inhibition or autophagy activation.

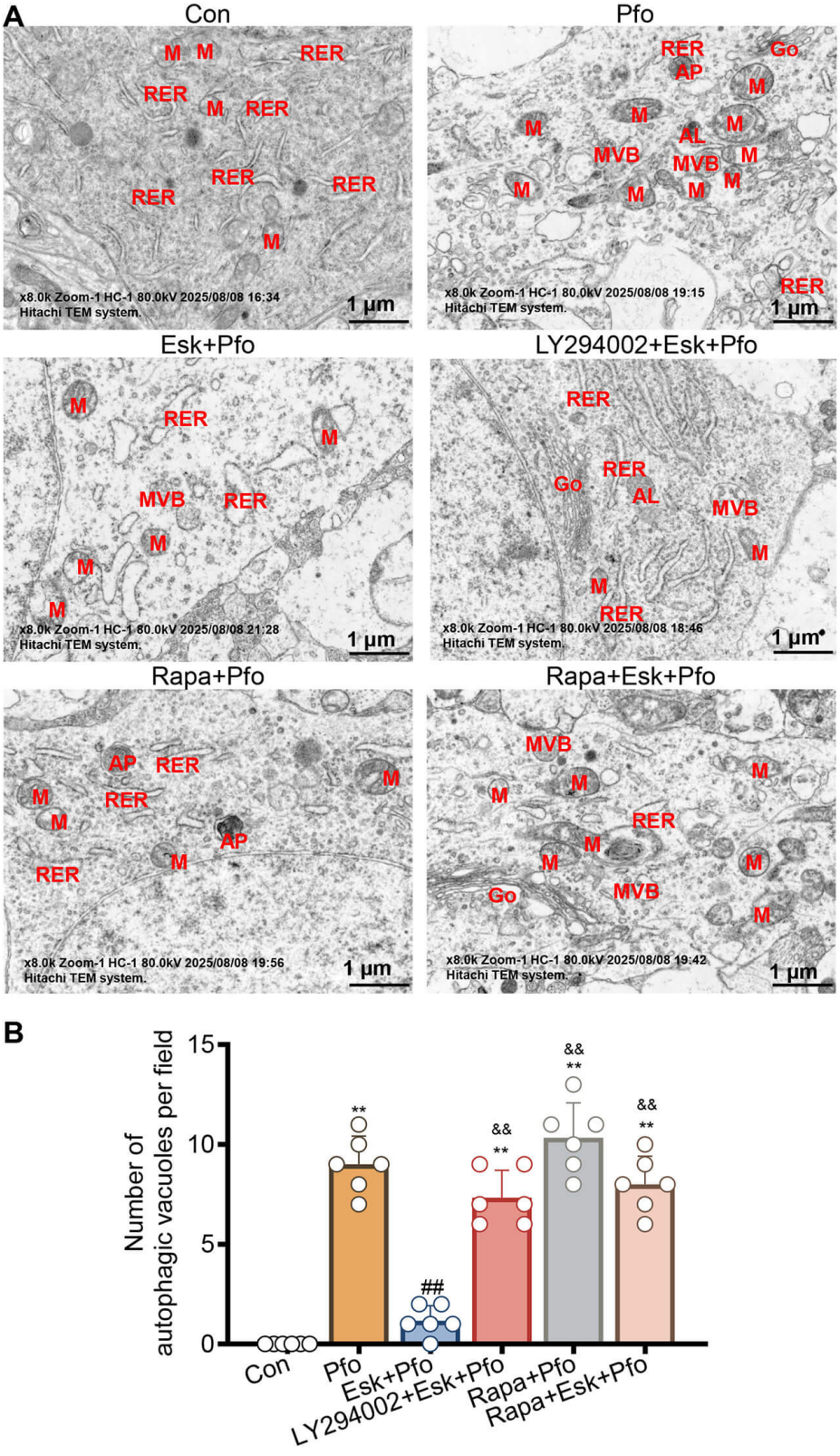

Fig. 3. Ultrastructural examination of hippocampal tissue. (A) Representative transmission electron microscopic images from each group. n = 6 rats per group. Key structures are indicated: mitochondria (M), rough endoplasmic reticulum (RER), multivesicular bodies (MVBs), Golgi apparatus (Go), autolysosomes (ALs), and autophagosomes (APs). Scale bar = 1 μm. (B) Quantitative analysis of autophagic vacuoles (AVs) per field, where AVs = APs + ALs. Data were presented as mean ± SD (n = 6 rats per group, with 5–10 fields per rat). $^{**}p < 0.01$ vs. Con; $^{\#\#}p < 0.01$ vs. Pfo; $^{\&\&}p < 0.01$ vs. Esk+Pfo. TEM, transmission electron microscopy.

3.3 Assessment of Ultrastructural Effects of Esketamine on Hippocampal Neurons and APs by TEM

TEM analysis revealed that esketamine preserved neuronal ultrastructure and reduced propofol-induced autophagic vacuole accumulation (Fig. 3A). The Con group displayed intact mitochondrial cristae and tightly attached ribosomes. In contrast, the Pfo group exhibited significant ultrastructural damage, including reduced and shortened mitochondrial cristae, dilation of the rough endoplasmic reticulum, and formation of APs, ALs, and MVBs. Esketamine markedly restored mitochondrial and endoplasmic reticulum integrity. Only occasional MVBs were observed, and no typical APs were identified, indicating an ultrastructural profile comparable to that of the controls. The protective effect of esketamine was abolished by co-administration of LY294002 or rapamycin. Both the LY294002+Esk+Pfo and Rapa+Esk+Pfo groups displayed ultrastructural damage similar to the Pfo group, with increased numbers of MVBs and ALs. Quantitative analysis confirmed that esketamine significantly attenuated the propofol-induced increase in autophagic vacuoles (AVs; defined as the sum of autophagosomes [APs] and autolysosomes [ALs]) per microscopic field, whereas this effect was abolished by treatment with LY294002 or rapamycin (Fig. 3B).

Collectively, these data demonstrated that esketamine preserved mitochondrial and endoplasmic reticulum integrity in propofol-exposed hippocampal neurons, and this protection was mediated by activation of the PI3K/Akt/mTOR signaling pathway, thereby limiting excessive autophagy.

3.4 Esketamine Attenuated Hippocampal Neuroinflammation

To assess neuroinflammatory responses, pro-inflammatory cytokine levels in hippocampal tissue were measured (Fig. 4). Relative to the Con group, hippocampal levels of IL-1β, IL-6, IL-18, and TNF-α (Fig. 4A–D) were significantly increased following propofol exposure (all $p < 0.01$). Esketamine significantly reduced levels of all four cytokines ($p < 0.01$), whereas PI3K inhibition or autophagy activation remarkably abolished this anti-inflammatory effect ($p < 0.01$). These results demonstrated that esketamine alleviated propofol-induced neuroinflammation through a mechanism dependent on PI3K pathway activation and autophagy suppression.

3.5 Esketamine Suppressed Excessive Autophagy via the PI3K/Akt/mTOR Pathway

3.5.1 Effects of Esketamine on Autophagy-Related Protein Expression in Hippocampal Neurons

The expression levels of key autophagy-related proteins in hippocampal tissue were assessed by Western blotting (Fig. 5, the original Western blotting images are provided in the **Supplementary Materials**). Propofol treatment significantly increased the LC3-II/LC3-I ratio and Beclin-1 expression level, while reduced autophagic substrate p62 level compared with the Con group, indicating abnormally activated autophagic flux. Treatment with esketamine significantly attenuated the autophagic response, which was characterized by lower LC3-II/LC3-I and Beclin-1 expression together with recovery of p62 levels.

In the Rapa+Esk+Pfo group, autophagy-related protein levels returned to those comparable to the Pfo group, indicating that rapamycin counteracted esketamine-mediated inhibition of autophagy. These results confirmed that esketamine effectively suppressed propofol-induced excessive autophagy, and this protective effect was reversed by exogenous autophagy activation.

3.5.2 PI3K/Akt/mTOR Signaling Mediated the Regulatory Effects of Esketamine on Autophagy

To identify the upstream mechanism by which esketamine regulates autophagy, the phosphorylation levels of key proteins in the PI3K/Akt/mTOR pathway were quantified (Fig. 6, the original Western blotting images are provided in the **Supplementary Materials**). The Pfo group showed significantly reduced p-PI3K, p-Akt, and p-mTOR levels compared with the Con group, indicating pathway inhibition. These were significantly restored by esketamine. However, co-administration of LY294002 completely abolished the restorative effect of esketamine, resulting in phosphorylation of these signaling proteins returning to values comparable with those observed in the Pfo group. Together, these findings showed that PI3K/Akt/mTOR activation mediated the suppression of excessive propofol-induced autophagy by esketamine.

3.5.3 Esketamine Alleviated Propofol-Induced Impairment of Autophagic Flux

The integrity of autophagic flux at the morphological level was assessed by immunofluorescence staining for AP marker LC3B and the lysosomal marker LAMP1 in hippocampal neurons (Fig. 7A). Propofol exposure markedly increased mean fluorescence intensities of both LC3B and LAMP1 (Fig. 7B,C), indicating a blockade at the lysosomal degradation stage of autophagic flux, with accumulation of APs and undegraded substrates. Esketamine significantly reduced signal intensities of both markers to approximately normal levels (Fig. 7B,C), reflecting that it not only reduced the excessive formation of APs, but also promoted AP-lysosome fusion and subsequent substrate degradation, thereby relieving the obstruction of autophagic flux.

Mechanistic validation experiments demonstrated that the restorative effect of esketamine on LC3B and LAMP1 signals was abolished by co-administration of either LY294002 or rapamycin. Both the LY294002+Esk+Pfo and Rapa+Esk+Pfo groups exhibited elevated expression levels of these markers, comparable to those found in the

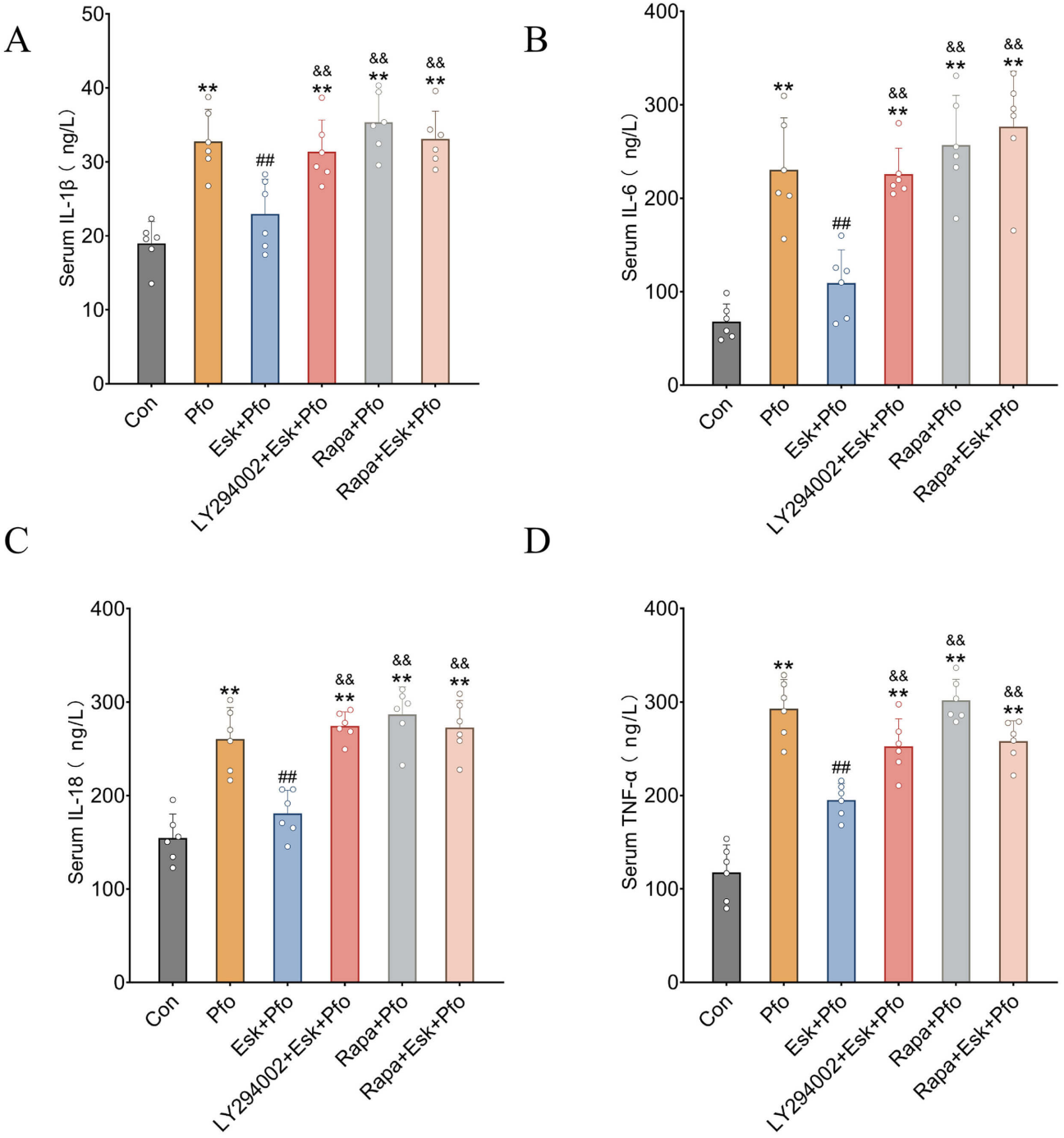

Fig. 4. Esketamine attenuates the inflammatory response in propofol-induced neurotoxicity. Concentrations of hippocampal inflammatory cytokines, including IL-1β (A), IL-6 (B), IL-18 (C), and TNF-α (D). Data were presented as mean ± SD (n = 6). $^{**}p < 0.01$ vs. Con; $^{\#\#}p < 0.01$ vs. Pfo; $^{\&\&}p < 0.01$ vs. Esk+Pfo. IL, interleukin; TNF-α, tumor necrosis factor-α.

Pfo group (Fig. 7B,C). These findings demonstrated that esketamine effectively alleviated propofol-induced disruption of autophagic flux by activating the PI3K pathway and suppressing excessive autophagy.

4. Discussion

This study revealed that repeated propofol anesthesia during the developmental period could induce long-term learning and memory impairments in rats. The underlying mechanism may involve suppression of the PI3K/Akt/mTOR signaling pathway and consequent excessive autophagy activation in hippocampal neurons. Importantly, it was revealed that esketamine could effectively counteract the excessive autophagy by activating the PI3K/Akt/mTOR pathway, thereby mitigating neuronal damage and cognitive dysfunction. These data highlighted

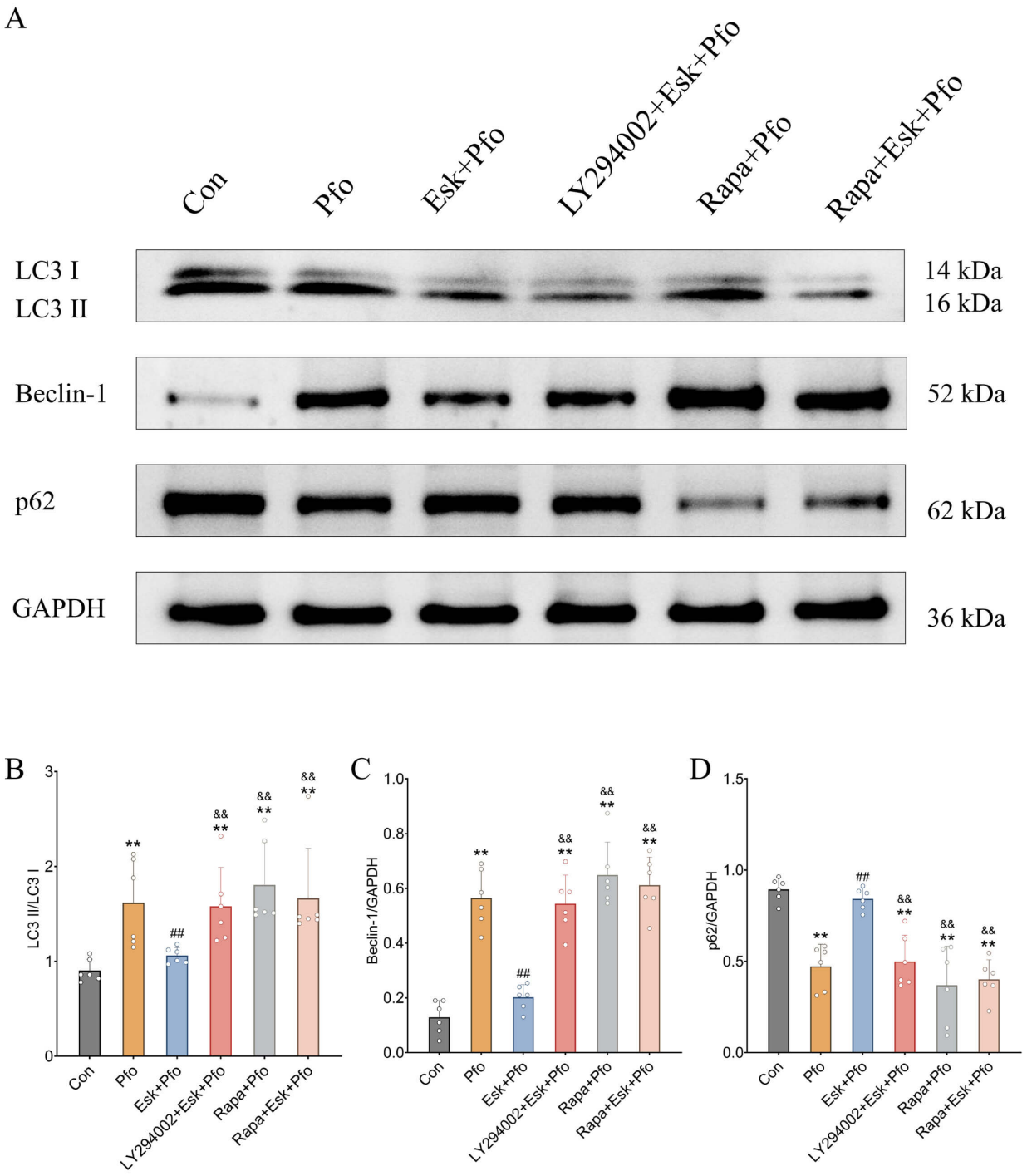

Fig. 5. Effects of esketamine on the expression levels of autophagy-related proteins. Representative Western blot bands (A) and quantitative analysis of LC3-II/LC3-I ratio (B), Beclin-1 (C), and p62 (D) in hippocampal tissues. Data were presented as mean ± SD (n = 6). $^{**}p < 0.01$ vs. Con; $^{\#\#}p < 0.01$ vs. Pfo; $^{\&\&}p < 0.01$ vs. Esk+Pfo. LC3, microtubule-associated protein 1A/1B-light chain 3.

the potential of esketamine as a promising therapeutic strategy for the prevention of propofol-induced neurotoxicity.

Both previous research and earlier studies conducted by our team have raised concerns regarding the potential neurotoxicity of propofol, an extensively utilized intravenous anesthetic, on the developing brain. Previous studies have demonstrated that repeated propofol exposure at the neonatal stage impaired hippocampal synaptic plasticity and long-term learning and memory capabilities [5,6,30]. Consistent with our previous findings, the current study confirmed that propofol administration could induce significant morphological abnormalities in hippocampal neurons, including disordered cellular arrangement, increased pyknosis, and worsened ultrastructural impairments, such

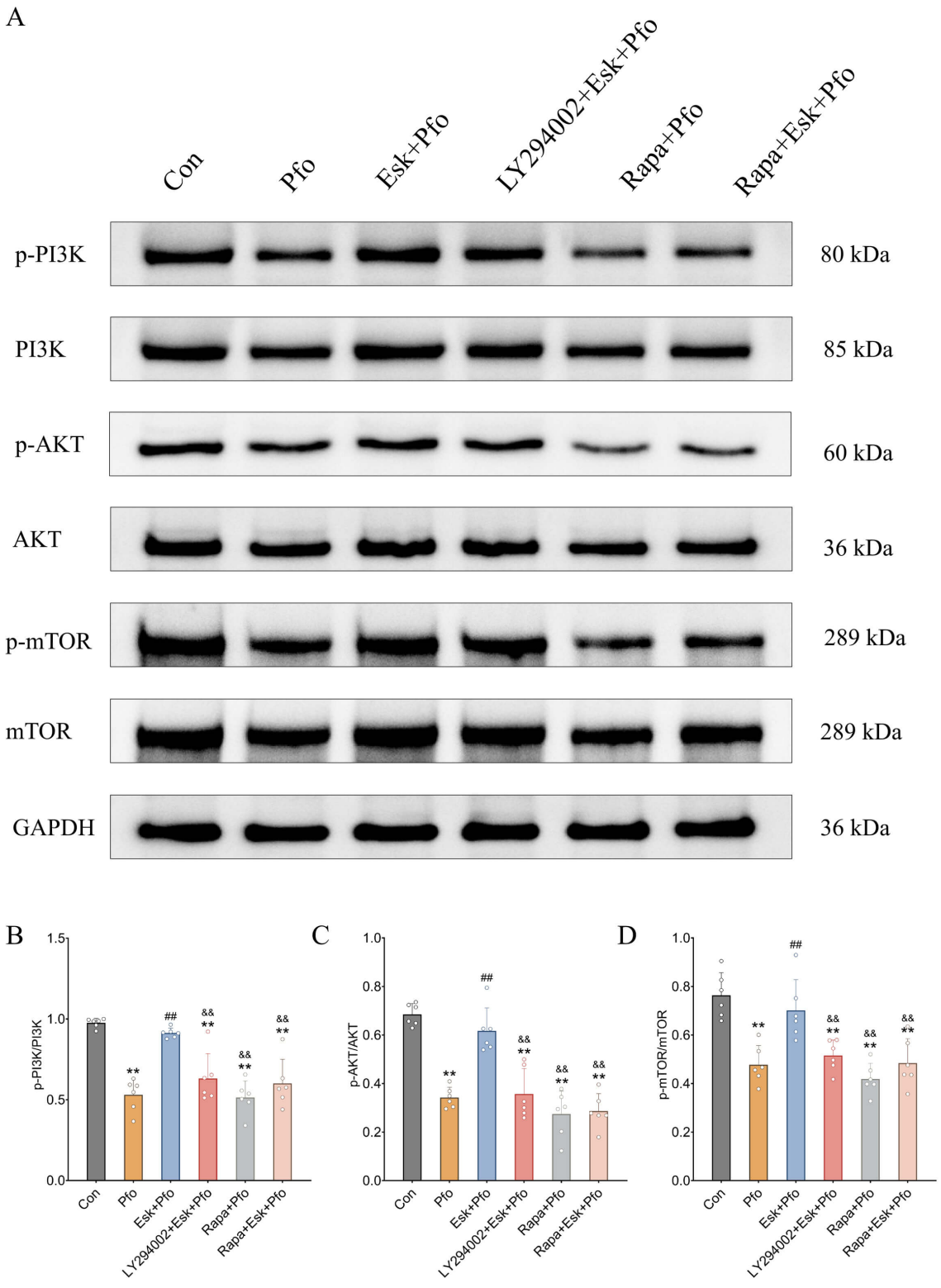

Fig. 6. Esketamine activates the PI3K/Akt/mTOR signaling pathway. Representative Western blot bands (A) and quantitative analysis of the p-PI3K/PI3K ratio (B), p-Akt/Akt ratio (C), and p-mTOR/mTOR ratio (D) in hippocampal tissues. The blots shown are representative of six independent biological replicates. The subtle band intensity differences in (A) were quantitatively confirmed in (B–D). Data were presented as mean ± SD (n = 6). $^{**}p < 0.01$ vs. Con; $^{\#\#}p < 0.01$ vs. Pfo; $^{\&\&}p < 0.01$ vs. Esk+Pfo. PI3K, phosphatidylinositol 3-kinase; Akt, protein kinase B; mTOR, mechanistic target of rapamycin.

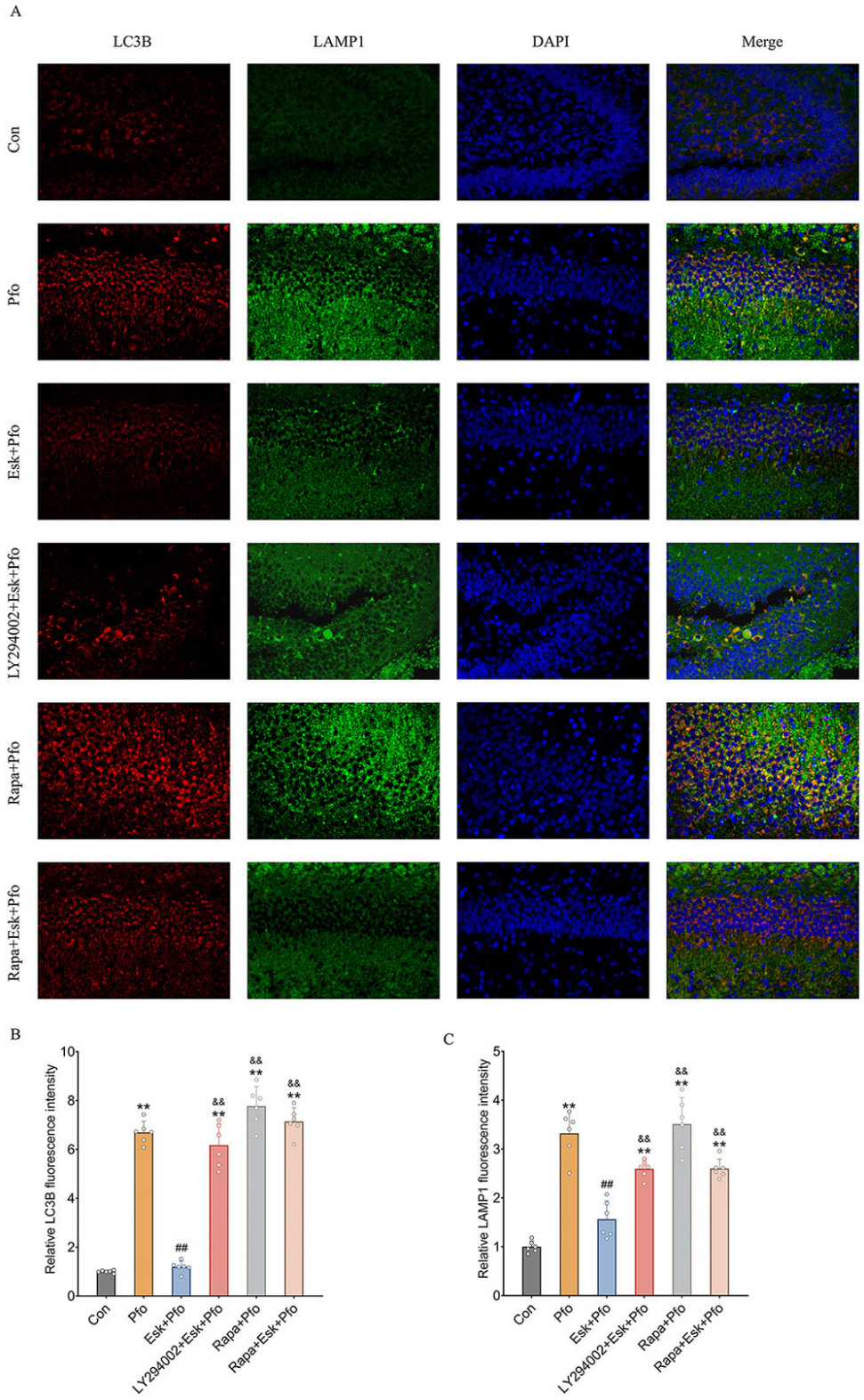

Fig. 7. Esketamine alleviates propofol-induced impairment of autophagic flux in hippocampal neurons. (A) Representative immunofluorescence images showing LC3B (red, AP marker), LAMP1 (green, lysosome marker), and DAPI (blue, nuclear staining) in the hippocampal CA1 region. n = 6 rats per group, with three non-overlapping fields per rat. Scale bar: 20 μm. (B) Quantitative analysis of relative LC3B fluorescence intensity (normalized to Control). (C) Quantitative analysis of relative LAMP1 fluorescence intensity (normalized to Control). Data were presented as mean ± SD (n = 6). $^{**}p < 0.01$ vs. Con; $^{\#\#}p < 0.01$ vs. Pfo; $^{\&\&}p < 0.01$ vs. Esk+Pfo. LAMP1, lysosomal-associated membrane protein 1; DAPI, 4′,6-diamidino-2-phenylindole.

as mitochondrial swelling, cristae fragmentation, and endoplasmic reticulum dilation. The results of behavioral tests further confirmed these cognitive deficits, as evidenced by an increased number of training trials required and a decreased correct response rate in the Y-maze test, along with prolonged escape latency and reduced platform crossings in the MWM test, collectively highlighting persistent memory and learning deficits in propofol-exposed rats.

Previous research has reported that propofol anesthesia could elevate the levels of pro-inflammatory cytokines, such as IL-18 and IL-1β, in the hippocampus, reflecting the contribution of neuroinflammation to the underlying neurotoxic process [7]. The present study further demonstrated that propofol could induce widespread neuroinflammatory responses in hippocampal tissue, as evidenced by significantly increased concentrations of IL-1β, IL-6, IL-18, and TNF-α. This inflammatory response was accompanied by remarkable autophagy activation, characterized by a higher LC3-II/LC3-I ratio, upregulated Beclin-1 expression level, and decreased autophagy substrate p62 level. Crucially, both TEM and semi-quantitative immunofluorescence analysis indicated a blockage at the lysosomal degradation stage of autophagic flux, leading to significant accumulation of APs and associated substrates. This disruption of autophagic flux integrity may represent a critical link in the pathogenesis of propofol-induced neurotoxicity.

However, existing literature presents inconsistent findings regarding propofol's modulation of autophagy, which may reflect the model-dependent nature of its effect. Sun et al. [31] found that propofol produced neuroprotection while inhibiting autophagy through Ca^{2+}/calcium/calmodulin-dependent protein kinase kinase beta (CaMKKβ)/AMP-activated protein kinase (AMPK)/mTOR signaling. However, this study was conducted in cultured cortical neurons under oxygen-glucose deprivation/reperfusion conditions rather than in neonatal animals *in vivo*, which is an important distinction from the present study. As highlighted in a comprehensive review by Yu et al. [32], propofol exerts both neuroprotective and neurotoxic effects depending on the experimental conditions, including the model system, dosage, exposure duration, and frequency of administration. In neonatal animals subjected to repeated propofol exposure, enhanced autophagy and neurotoxicity have been more consistently reported [32]. Consistent with findings of the present study, long-term propofol has been shown to reduce the activity of neurons and cause developmental neurotoxicity through excessive autophagy [33], further supporting the conclusions of the present study.

Autophagy is a cellular process crucial for maintaining homeostasis through the formation of APs that encapsulate and degrade non-essential or damaged components [34]. The expression levels of LC3B and LAMP1, serving as marker proteins for APs and lysosomes, respectively, can reflect the integrity of autophagic flux. The semi-quantitative immunofluorescence analysis revealed significantly increased mean fluorescence intensities of both LC3B and LAMP1 following propofol treatment, indicating potential impairment at the AP-lysosome fusion stage, leading to the compromised clearance of autophagic substrates. Similarly, Livieri et al. [35] regarded LC3B and LAMP2A as key indicators to evaluate autophagic flux integrity in their traumatic brain injury study. Furthermore, Beclin-1, p62, and LC3B are widely recognized as core proteins in the autophagy process [36]. Beclin-1 regulates AP formation [37], LC3B-II binds to autophagosomal membranes reflecting autophagic activity [38], and p62 accumulation, serving as a selective autophagic receptor, typically indicates impaired autophagic degradation [39]. In the present study, the propofol group exhibited increased Beclin-1 expression level and LC3B-II/LC3B-I ratio, alongside decreased p62 level, accompanied by synchronized elevation of LC3B and LAMP1 fluorescence intensities, collectively demonstrating both autophagy activation and blockade at the degradation stage of autophagic flux. These findings indicate that propofol-induced neurotoxicity is closely associated with abnormally enhanced autophagy, reflecting that suppressing excessive autophagy could represent a potential strategy for mitigating its neurotoxic effects.

Previous research has confirmed that esketamine could prevent propofol-induced neurotoxicity through anti-inflammatory mechanisms [20]. In the present study, esketamine pretreatment not only significantly improved cognitive performance in both Y-maze and MWM tests, but also effectively alleviated morphological damage and ultrastructural abnormalities in hippocampal neurons. Furthermore, it was revealed that its protective effects were closely associated with the regulation of autophagy. Esketamine pretreatment significantly reduced the LC3-II/LC3-I ratio and Beclin-1 expression level, while increasing p62 level, indicating suppression of the autophagic activity. Semi-quantitative immunofluorescence analysis demonstrated reduced mean fluorescence intensities of both LC3B and LAMP1, reflecting diminished AP accumulation and restored integrity of autophagic flux. To verify the role of autophagy inhibition in its protective mechanism, the autophagy activator rapamycin was utilized. The results indicated that rapamycin treatment abolished the benefits of esketamine, as evidenced by significantly increased pro-inflammatory cytokine release, restoration of autophagy marker expression similar to that in the propofol group, and exacerbation of brain injury. These findings strongly confirm that the neuroprotective effects of esketamine depend on its ability to suppress excessive autophagy.

According to these findings, the upstream signaling mechanisms were further investigated through which esketamine could regulate autophagy. The PI3K/Akt/mTOR pathway is a well-established negative regulatory signaling pathway of autophagy, whose activation suppresses

autophagic activity and maintains neuronal homeostasis [22]. Previous studies have confirmed that the enhanced autophagy following repeated propofol anesthesia may be detrimental to neurons, while mTOR activation can mitigate this excessive autophagic response [40]. In the present study, propofol-related brain injury was accompanied by significant reductions in p-PI3K, p-Akt, and p-mTOR, in parallel with downstream activation of autophagy. Esketamine pretreatment effectively restored the activity of this signaling pathway. Crucially, the PI3K inhibitor LY294002 completely abolished both esketamine-mediated activation of the PI3K/Akt/mTOR pathway and its subsequent suppressive effects on autophagy and neuroprotection. These results collectively indicated that esketamine could suppress propofol-induced excessive autophagy, specifically by activating the PI3K/Akt/mTOR signaling pathway. However, the mechanism by which esketamine initiates PI3K pathway was not determined here and has rarely been addressed in previous reports. This represents a key scientific question that warrants further investigation in future studies. In addition, it should be noted that under certain conditions, NMDA receptor antagonism can itself upregulate autophagy, which would be expected to counteract the autophagy-suppressing effects found in this study [41]. Nevertheless, cotreatment with esketamine consistently activated PI3K/Akt/mTOR pathway and suppressed excessive autophagy, indicating that its effects on this model favored autophagy inhibition despite any potential NMDA antagonism-driven autophagic induction. This apparent paradox highlights the complexity of autophagy regulation in the developing brain. The respective contributions of NMDA receptor antagonism and PI3K/Akt/mTOR pathway activation to the observed suppression of autophagy have yet to be fully clarified.

This study has several limitations. First, no esketamine-alone group was included, limiting the ability to distinguish its independent effects from its interaction with propofol, although previous research has not shown cognitive effects at the dose used [20]. Second, only esketamine was evaluated; it remains elusive whether the observed neuroprotection is specific to esketamine or shared among other non-competitive NMDA receptor antagonists, such as phencyclidine or dextromethorphan. Third, the study did not directly isolate NMDA receptor-dependent mechanisms, and the contribution of this pathway could not be definitively determined. Additionally, neither the LY294002-alone nor the rapamycin-alone group was included, thereby limiting mechanistic interpretation of their independent effects. Fourth, the quantification methods used for hippocampal CA1 neurons and APs in the TEM analyses provided only semi-quantitative density estimates rather than absolute numbers. Because stereological methods were not employed, the analyses do not yield unbiased estimates of organelle number per unit volume or per cell, and this should be considered when interpreting the quantitative findings. Furthermore, although juvenile rats provide a valuable experimental model for developmental neurotoxicity, species differences in brain development, phar-

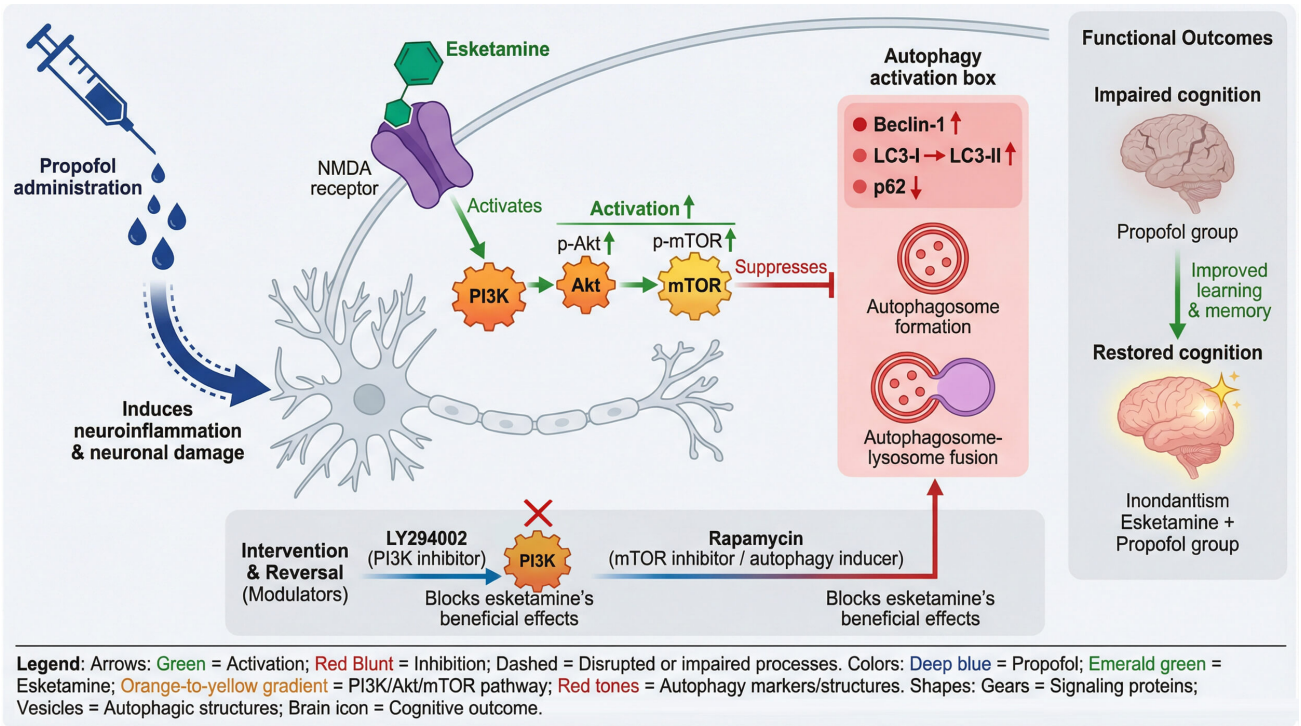

Fig. 8. Schematic diagram of the proposed mechanism. Green arrows indicate activation; red blunt arrows indicate inhibition/suppression; and blue arrows indicate blockade of esketamine's beneficial effects.

macokinetics, and anesthetic responses limit the direct extrapolation of these findings to pediatric clinical practice. The neuroprotective effects of esketamine observed in this study should be validated in additional preclinical models and clinical studies. Moreover, this study evaluated only the short-term effects of esketamine following propofol exposure and did not assess its long-term safety or potential consequences on neurodevelopment and cognitive function. Future studies incorporating long-term histopathological and molecular assessments are warranted to establish the durability and safety of esketamine treatment. Lastly, the absence of autophagy-inhibitor controls, such as 3-methyladenine or chloroquine, precludes definitive confirmation of a causal relationship between esketamine-mediated autophagy modulation and neuroprotection. Future studies should incorporate both pharmacological autophagy inhibitors and activators to more accurately indicate the directional contribution of autophagy to the neuroprotective effects of esketamine.

5. Conclusions

This study identified a potential mechanism through which esketamine alleviated persistent learning and memory deficits in juvenile rats following repeated propofol anesthesia (Fig. 8). It was revealed that repeated propofol anesthesia produced cognitive deficits accompanied by PI3K/Akt/mTOR pathway inhibition and hippocampal autophagic dysfunction, including excessive activation and impaired flux. Pretreatment with esketamine restored PI3K/Akt/mTOR phosphorylation, suppressed excessive autophagy, improved the clearance of damaged organelles, and ultimately protected neuronal structure and cognitive function. These findings provide novel theoretical insights and potential therapeutic targets for the clinical prevention of anesthesia-induced neurotoxicity.

Abbreviations

Akt, protein kinase B; ALs, autolysosomes; APs, autophagosomes; AVs, autophagic vacuoles; ARRIVE, animal research: reporting of *in vivo* experiments; CA1, Cornu Ammonis area 1; Con, Control; DAPI, 4′,6-diamidino-2-phenylindole; ELISA, enzyme-linked immunosorbent assay; Esk, Esketamine; GAPDH, glyceraldehyde-3-phosphate dehydrogenase; H&E, hematoxylin and eosin; HRP, horseradish peroxidase; i.p., intraperitoneal; IL-1β, interleukin-1 beta; IL-6, interleukin-6; IL-18, interleukin-18; LAMP1, lysosomal-associated membrane protein 1; LC3, microtubule-associated protein 1A/1B-light chain 3; mTOR, mechanistic target of rapamycin; MVBs, multivesicular bodies; MWM, morris water maze; NIH, National Institutes of Health; NMDA, N-methyl-D-aspartate; P7, postnatal day 7; Pfo, Propofol; PI3K, phosphatidylinositol 3-kinase; Rapa, Rapamycin; RER, rough endoplasmic reticulum; SD, standard deviation; SDS-PAGE, sodium dodecyl sulfate-polyacrylamide gel electrophoresis; TBST, tris-buffered saline with tween; TEM, transmission electron microscopy; TNF-α, tumor necrosis factor-alpha; TSA, tyramide signal amplification.

Availability of Data and Materials

All data relevant to the findings of this study are available from the corresponding author upon reasonable request.

Author Contributions

YW: Conceptualization, Methodology, Investigation, Formal analysis, Writing – Original Draft, Writing – Review & Editing, Funding acquisition. YL: Investigation, Data Curation, Validation. ZC: Resources, Software, Visualization. XZ: Investigation, Methodology. NQ: Data Curation, Formal analysis. XC: Supervision, Validation. GX: Supervision, Validation, Funding acquisition, Writing – Review & Editing, Project administration, Resources. All authors contributed to editorial changes in the manuscript. All authors have read and approved the final version of the manuscript. All authors have participated sufficiently in the work and agreed to be accountable for all aspects of the work.

Ethics Approval and Consent to Participate

All animals were given ad libitum access to food and water. All experimental procedures were approved by the Animal Ethics Committee of the People's Hospital of Xinjiang Uygur Autonomous Region (Approval No. SYDW2023090702), and they were conducted in accordance with the ARRIVE 2.0 guidelines and the National Institutes of Health (NIH) standards for Care and Use of laboratory animal welfare.

Acknowledgment

We would like to express my gratitude to all those who helped me during the writing of this manuscript.

Funding

This study was supported by the Natural Science Foundation of Xinjiang Uygur Autonomous Region (Grant No. 2024D01C287), the In-hospital Project of People's Hospital of Xinjiang Uygur Autonomous Region (Grant No. 20230105), and the "Tianshan Talent" Training Program for Medical and Health High-level Talents in Xinjiang (Grant No. TSYC202401A003). The funders had no role in study design, data collection and analysis, decision to publish, or preparation of the manuscript.

Conflicts of Interest

The authors declare no conflicts of interest.

Supplementary Material

Supplementary material associated with this article can be found, in the online version, at https://doi.org/10.31083/JIN50741.

References

[1] Wong-Kee-You AMB, Loveridge-Easther C, Mueller C, Simon N, Good WV. The impact of early exposure to general anesthesia on visual and neurocognitive development. Survey of Ophthalmology. 2023; 68: 539–555. https://doi.org/10.1016/j.survophthal.2022.08.006

[2] Yan J, Xu J, Wang F, Gao Y, Qi C, Chen T, et al. The Relationship between Early Exposure to General Anesthesia and Neurobehavioral Deficits. Developmental Neuroscience. 2025; 47: 383–399. https://doi.org/10.1159/000542005

[3] Jia X, Tan S, Qin Y, Wei Y, Jiang Y, Pan S, et al. Experiencing anesthesia and surgery early in life impairs cognitive and behavioral development. Frontiers in Neuroscience. 2024; 18: 1406172. https://doi.org/10.3389/fnins.2024.1406172

[4] Grabowski J, Goldin A, Arthur LG, Beres AL, Guner YS, Hu YY, et al. The effects of early anesthesia on neurodevelopment: A systematic review. Journal of Pediatric Surgery. 2021; 56: 851–861. https://doi.org/10.1016/j.jpedsurg.2021.01.002

[5] Ma LH, Wan J, Yan J, Wang N, Liu YP, Wang HB, et al. Hippocampal SIRT1-Mediated Synaptic Plasticity and Glutamatergic Neuronal Excitability Are Involved in Prolonged Cognitive Dysfunction of Neonatal Rats Exposed to Propofol. Molecular Neurobiology. 2022; 59: 1938–1953. https://doi.org/10.1007/s12035-021-02684-4

[6] Wan J, Shen CM, Wang Y, Wu QZ, Wang YL, Liu Q, et al. Repeated exposure to propofol in the neonatal period impairs hippocampal synaptic plasticity and the recognition function of rats in adulthood. Brain Research Bulletin. 2021; 169: 63–72. https://doi.org/10.1016/j.brainresbull.2021.01.007

[7] Zhang Z, Chen H, Han L, Liu K, Du S, Gao R. Inhibition of the NLRP3/caspase-1 cascade related pyroptosis relieved propofol-induced neuroinflammation and cognitive impairment in developing rats. Free Radical Biology & Medicine. 2024; 225: 87–97. https://doi.org/10.1016/j.freeradbiomed.2024.09.038

[8] Yang N, Li Z, Han D, Mi X, Tian M, Liu T, et al. Autophagy prevents hippocampal α-synuclein oligomerization and early cognitive dysfunction after anesthesia/surgery in aged rats. Aging. 2020; 12: 7262–7281. https://doi.org/10.18632/aging.103074

[9] Pandey K, Yu XW, Steinmetz A, Alberini CM. Autophagy coupled to translation is required for long-term memory. Autophagy. 2021; 17: 1614–1635. https://doi.org/10.1080/15548627.2020.1775393

[10] Khoury R, Saad J, Jabre V, Ghayad LM, Khalifeh M, Houbeika R, et al. Autophagy regulates the release of exercise factors and their beneficial effects on spatial memory recall. Heliyon. 2023; 9: e14705. https://doi.org/10.1016/j.heliyon.2023.e14705

[11] Xu X, Yang J, Jia Q, Hu Q, Liu H. Protective effects of dexmedetomidine against propofol-induced memory impairment in developing rat involved Src and RARα. Human & Experimental Toxicology. 2025; 44: 9603271251336467. https://doi.org/10.1177/09603271251336467

[12] Dang X, Huan X, Du X, Chen X, Bi M, Yan C, et al. Correlation of Ferroptosis and Other Types of Cell Death in Neurodegenerative Diseases. Neuroscience Bulletin. 2022; 38: 938–952. https://doi.org/10.1007/s12264-022-00861-6

[13] Li H, Deng J, Liu T, Zhang Y. Clinical applications of esketamine: Current status and future perspectives. The Journal of International Medical Research. 2026; 54: 3000605261432759. https://doi.org/10.1177/03000605261432759

[14] Zhao L, Li Z, Jin B, Hou N, Yang H. Safety and efficacy of low-dose esketamine in laparoscopic cholecystectomy: a prospective, double-blind randomized controlled trial. BMC Anesthesiology. 2024; 24: 47. https://doi.org/10.1186/s12871-024-02429-5

[15] Huang X, Lin F, Chen Q, Hu X. Safety and efficacy of the combination of esketamine and propofol in procedural sedation/analgesia: a systematic review and meta-analysis. Minerva Anestesiologica. 2023; 89: 680–689. https://doi.org/10.23736/S0375-9393.23.17100-8

[16] Wang T, Weng H, Zhou H, Yang Z, Tian Z, Xi B, et al. Esketamine alleviates postoperative depression-like behavior through anti-inflammatory actions in mouse prefrontal cortex. Journal of Affective Disorders. 2022; 307: 97–107. https://doi.org/10.1016/j.jad.2022.03.072

[17] Beyeler A. Do antidepressants restore lost synapses? Science (New York, N.Y.). 2019; 364: 129–130. https://doi.org/10.1126/science.aax0719

[18] Duan WY, Peng K, Qin HM, Li BM, Xu YX, Wang DJ, et al. Esketamine accelerates emergence from isoflurane general anaesthesia by activating the paraventricular thalamus glutamatergic neurones in mice. British Journal of Anaesthesia. 2024; 132: 334–342. https://doi.org/10.1016/j.bja.2023.10.038

[19] Tang Y, Liu Y, Zhou H, Lu H, Zhang Y, Hua J, et al. Esketamine is neuroprotective against traumatic brain injury through its modulation of autophagy and oxidative stress via AMPK/mTOR-dependent TFEB nuclear translocation. Experimental Neurology. 2023; 366: 114436. https://doi.org/10.1016/j.expneurol.2023.114436

[20] Xu G, Wang Y, Chen Z, Zhang Y, Zhang X, Zhang G. Esketamine improves propofol-induced brain injury and cognitive impairment in rats. Translational Neuroscience. 2022; 13: 430–439. https://doi.org/10.1515/tnsci-2022-0251

[21] Zhang J, Xu G, Wang X, Qiao L. Investigating the Mechanisms of Esketamine in Treating Propofol-Induced Cognitive Impairment in Elderly Rats. Discovery Medicine. 2025; 37: 695–705. https://doi.org/10.24976/Discov.Med.202537195.60

[22] Li R, Zheng Y, Zhang J, Zhou Y, Fan X. Gomisin N attenuated cerebral ischemia-reperfusion injury through inhibition of autophagy by activating the PI3K/AKT/mTOR pathway. Phytomedicine : International Journal of Phytotherapy and Phytopharmacology. 2023; 110: 154644. https://doi.org/10.1016/j.phymed.2023.154644

[23] Han J, Zhang X, Xia L, Liao O, Li Q. S-ketamine promotes autophagy and alleviates neuropathic pain by inhibiting PI3K/Akt/mTOR signaling pathway. Molecular & Cellular Toxicology. 2023; 19: 81–88. https://doi.org/10.1007/s13273-022-00243-z

[24] Zhong Y, Chen J, Li L, Qin Y, Wei Y, Pan S, et al. PKA-CREB-BDNF signaling pathway mediates propofol-induced long-term learning and memory impairment in hippocampus of rats. Brain Research. 2018; 1691: 64–74. https://doi.org/10.1016/j.brainres.2018.04.022

[25] Li J, Wang K, Liu M, He J, Zhang H, Liu H. Dexmedetomidine alleviates cerebral ischemia-reperfusion injury via inhibiting autophagy through PI3K/Akt/mTOR pathway. Journal of Molecular Histology. 2023; 54: 173–181. https://doi.org/10.1007/s10735-023-10120-1

[26] Zheng G, Wang L, Li X, Niu X, Xu G, Lv P. Rapamycin alleviates cognitive impairment in murine vascular dementia: The enhancement of mitophagy by PI3K/AKT/mTOR axis. Tissue & Cell. 2021; 69: 101481. https://doi.org/10.1016/j.tice.2020.101481

[27] Cleal M, Fontana BD, Ranson DC, McBride SD, Swinny JD, Redhead ES, et al. The Free-movement pattern Y-maze: A cross-species measure of working memory and executive function. Behavior Research Methods. 2021; 53: 536–557. https://doi.org/

10.3758/s13428-020-01452-x
[28] Howe CL, Lafrance-Corey RG, Sundsbak RS, Sauer BM, Lafrance SJ, Buenz EJ, et al. Hippocampal protection in mice with an attenuated inflammatory monocyte response to acute CNS picornavirus infection. Scientific Reports. 2012; 2: 545. https://doi.org/10.1038/srep00545
[29] Klionsky DJ, Abdel-Aziz AK, Abdelfatah S, Abdellatif M, Abdoli A, Abel S, et al. Guidelines for the use and interpretation of assays for monitoring autophagy (4th edition)[1]. Autophagy. 2021; 17: 1–382. https://doi.org/10.1080/15548627.2020.1797280
[30] Dai QD, Wu KS, Xu LP, Zhang Y, Lin N, Jiang Y, et al. Toll-Like Receptor 4 Deficiency Ameliorates Propofol-Induced Impairments of Cognitive Function and Synaptic Plasticity in Young Mice. Molecular Neurobiology. 2024; 61: 519–532. https://doi.org/10.1007/s12035-023-03606-2
[31] Sun B, Ou H, Ren F, Huan Y, Zhong T, Gao M, et al. Propofol inhibited autophagy through Ca^{2+}/CaMKKβ/AMPK/mTOR pathway in OGD/R-induced neuron injury. Molecular Medicine (Cambridge, Mass.). 2018; 24: 58. https://doi.org/10.1186/s10020-018-0054-1
[32] Yu S, Liao J, Lin X, Luo Y, Lu G. Crucial role of autophagy in propofol-treated neurological diseases: a comprehensive review. Frontiers in Cellular Neuroscience. 2023; 17: 1274727. https://doi.org/10.3389/fncel.2023.1274727
[33] Qiao H, Li Y, Xu Z, Li W, Fu Z, Wang Y, et al. Propofol Affects Neurodegeneration and Neurogenesis by Regulation of Autophagy via Effects on Intracellular Calcium Homeostasis. Anesthesiology. 2017; 127: 490–501. https://doi.org/10.1097/ALN.0000000000001730
[34] Liang Y. Phagophore-lysosome/vacuole fusion in mutant yeast and mammalian cells. Autophagy. 2023; 19: 2595–2600. https://doi.org/10.1080/15548627.2023.2205272
[35] Livieri T, Alfieri L, Giacomello E, Alempijević D, Petrovic T, Kolev YG, et al. Traumatic brain injury and autophagy: a pilot study about the immunohistochemical expression of LC3B, Beclin 1, p62, and LAMP2A in human autoptic samples. Frontiers in Molecular Neuroscience. 2025; 18: 1562954. https://doi.org/10.3389/fnmol.2025.1562954
[36] Lin Z, Li LY, Chen L, Jin C, Li Y, Yang L, et al. Lonicerin promotes wound healing in diabetic rats by enhancing blood vessel regeneration through Sirt1-mediated autophagy. Acta Pharmacologica Sinica. 2024; 45: 815–830. https://doi.org/10.1038/s41401-023-01193-5
[37] Hu D, Huo Y, Xue Y, Feng H, Sun W, Wang H, et al. Clinical application of autophagy proteins as prognostic biomarkers in colorectal cancer: a meta-analysis. Future Oncology (London, England). 2022; 18: 3537–3549. https://doi.org/10.2217/fon-2022-0458
[38] Hwang HJ, Kim YK. The role of LC3B in autophagy as an RNA-binding protein. Autophagy. 2023; 19: 1028–1030. https://doi.org/10.1080/15548627.2022.2111083
[39] Rathore AS, Singh SS, Birla H, Zahra W, Keshri PK, Dilnashin H, et al. Curcumin Modulates p62-Keap1-Nrf2-Mediated Autophagy in Rotenone-Induced Parkinson's Disease Mouse Models. ACS Chemical Neuroscience. 2023; 14: 1412–1423. https://doi.org/10.1021/acschemneuro.2c00706
[40] Zhang T, Ji D, Sun J, Song J, Nie L, Sun N. NPAS4 suppresses propofol-induced neurotoxicity by inhibiting autophagy in hippocampal neuronal cells. Archives of Biochemistry and Biophysics. 2021; 711: 109018. https://doi.org/10.1016/j.abb.2021.109018
[41] Companys-Alemany J, Turcu AL, Schneider M, Müller CE, Vázquez S, Griñán-Ferré C, et al. NMDA receptor antagonists reduce amyloid-β deposition by modulating calpain-1 signaling and autophagy, rescuing cognitive impairment in 5XFAD mice. Cellular and Molecular Life Sciences. 2022; 79: 408. https://doi.org/10.1007/s00018-022-04438-4